Journal of Astronomical Telescopes, Instruments, and Systems

AstronomicalTelescopes.SPIEDigitalLibrary.org

Ultralightweight x-ray telescope missions: ORBIS and GEO-X

Yuichiro Ezoe
Yoshizumi Miyoshi
Satoshi Kasahara
Tomoki Kimura
Kumi Ishikawa
Masaki Fujimoto
Kazuhisa Mitsuda
Hironori Sahara
Naoki Isobe
Hiroshi Nakajima
Takaya Ohashi
Harunori Nagata
Ryu Funase
Munetaka Ueno
Graziella Branduardi-Raymont

Yuichiro Ezoe, Yoshizumi Miyoshi, Satoshi Kasahara, Tomoki Kimura, Kumi Ishikawa, Masaki Fujimoto, Kazuhisa Mitsuda, Hironori Sahara, Naoki Isobe, Hiroshi Nakajima, Takaya Ohashi, Harunori Nagata, Ryu Funase, Munetaka Ueno, Graziella Branduardi-Raymont, "Ultralightweight x-ray telescope missions: ORBIS and GEO-X," *J. Astron. Telesc. Instrum. Syst.* **4**(4), 046001 (2018), doi: 10.1117/1.JATIS.4.4.046001.

Ultralightweight x-ray telescope missions: ORBIS and GEO-X

Yuichiro Ezoe,[a,*] Yoshizumi Miyoshi,[b] Satoshi Kasahara,[c] Tomoki Kimura,[d] Kumi Ishikawa,[e] Masaki Fujimoto,[e] Kazuhisa Mitsuda,[e] Hironori Sahara,[a] Naoki Isobe,[e] Hiroshi Nakajima,[f] Takaya Ohashi,[a] Harunori Nagata,[g] Ryu Funase,[c] Munetaka Ueno,[h] and Graziella Branduardi-Raymont[i]

[a]Tokyo Metropolitan University, Tokyo, Japan
[b]Nagoya University, Nagoya, Japan
[c]University of Tokyo, Tokyo, Japan
[d]Tohoku University, Sendai, Japan
[e]Institute of Space and Astronautical Science, Japan Aerospace Exploration Agency, Sagamihara, Japan
[f]Kanto Gakuin University, Yokohama, Japan
[g]Hokkaido University, Sapporo, Japan
[h]Kobe University, Kobe, Japan
[i]University College London, Mullard Space Science Laboratory, Surrey, United Kingdom

Abstract. Toward an era of x-ray astronomy, next-generation x-ray optics are indispensable. To meet a demand for telescopes lighter than the foil optics but with a better angular resolution <1 arcmin, we are developing micropore x-ray optics based on micromaching technologies. Using sidewalls of micropores through a thin silicon wafer, this type can be the lightest x-ray telescope ever achieved. Two Japanese missions, ORBIS and GEO-X, will carry this telescope. ORBIS is a small x-ray astronomy mission to monitor supermassive blackholes, while GEO-X is a small exploration mission of the Earth's magnetosphere. Both missions need an ultralightweight (<1 kg) telescope with moderately good angular resolution (<10 arcmin) at an extremely short focal length (<30 cm). We plan to demonstrate this type of telescope in these two missions around 2020. [DOI: 10.1117/1.JATIS.4.4.046001]

Keywords: x-ray telescope; small satellite; ORBIS; GEO-X.

Paper 18054 received Jul. 12, 2018; accepted for publication Sep. 5, 2018; published online Oct. 4, 2018.

1 Introduction

X-ray telescopes are essential for future x-ray astronomy. Toward a new era of x-ray astronomy, next-generation x-ray optics are needed. Three different methods have been established in past x-ray missions: direct polishing of glass, replication of thin shells from an accurately shaped mandrel, and thin foils bent to a conical approximation of a Wolter type-I geometry. As shown in Fig. 1, there is a well-known trade-off relation between the angular resolution and the mass normalized by the effective area among these three methods.[1] In order to break this relation, new mirror fabrication methods are demanded.

There is an obvious need for telescopes as light as the foil optics but with <10 arcsec angular resolution, which is ×10 better than the foil optics. Silicon pore optics, precision polishing of single-crystal silicon, slumping of glass sheets, and adjustable optics with piezo stress are being developed for this purpose (e.g., Refs. 2–4). Such technologies are especially important for large x-ray observatories such as Athena and Lynx.

There is another demand for different telescopes that are lighter than the foil optics but have a comparable or better angular resolution of <1 arcmin. Potential applications are an all-sky monitor to cover a large fraction of the sky with focusing x-ray telescopes, small/medium class astronomy satellites, and solar system exploration missions.

*Address all correspondence to: Yuichiro Ezoe; E-mail: ezoe@tmu.ac.jp

For these two purposes, micropore x-ray optics are now considered as good candidates. Sidewalls of micropores through a thin substrate are utilized for x-ray mirrors. If we shrink the size of the mirrors by a factor of C, the mirror weight decreases by C^3. To keep the same effective area, we have to increase the mirror number by C^2. Consequently, the telescope weight will decrease by $C^{3-2} = C^1$. Therefore, using micropores with a width of the order of $10 \sim 100$ μm for x-ray mirrors, the micropore optics can be light in weight.[5]

Three types of micropore optics have been proposed and are being developed. The first type is microchannel plate optics (MCP) made of glass fibers.[6,7] Sidewalls of square pores are utilized for x-ray mirrors. A spherically bent glass plate with numerous micropores works as lobster-eye optics. By stacking two plates, a Wolter type-I optic is also fabricated for the ESA's BepiColombo mission.[8] The second type is the silicon pore optics, called SPO.[1,2,7] A thin silicon wafer diced into rectangles is wedged and stacked onto another wafer so that the surface of the wafer is utilized for x-ray mirrors. This type is employed in the ESA's large x-ray observatory, Athena.

As a third type, we have invented and are developing what we call MEMS x-ray optics.[5,9–14] MEMS stands for microelectromechanical systems. We apply micromachining technologies for the micropore x-ray optics. To date, we have demonstrated x-ray reflection and imaging with various MEMS techniques. In this paper, we introduce two new Japanese small mission plans, Orbiting Binary Blackhole Investigation Satellite (ORBIS) and GEO-X, which will carry the MEMS x-ray optics. We then introduce the MEMS x-ray optics.

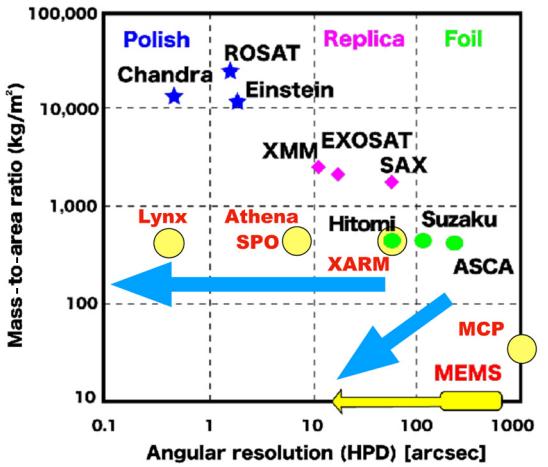

Fig. 1 Performances of past and future x-ray telescopes. A horizontal axis is the angular resolution in half power diameter (HPD), while a vertical axis is a telescope mass normalized by an effective area at 1 keV. Stars, diamonds, and green circles represent x-ray telescopes onboard past space missions. Yellow circles (with outlined circumferences) represent are required performances in future missions or expected performances of micropore x-ray optics. Blue arrows indicate the two major demands in future missions. A goal of our MEMS x-ray optics is shown in a yellow arrow.

2 Small Missions

2.1 *ORBIS*

ORBIS is a university-built astronomy satellite led by Tokyo Metropolitan University in collaboration with ISAS/JAXA, Kanto Gakuin University, Kansei Gakuin University, Osaka University, and Meisei University.[15] Its scientific objective is to search for a signature of a binary black hole (BBH) by observing a specific active galactic nucleus (AGN) continuously for a long time (∼1 year).

In spite of detections of gravitational waves from intermediate mass BBHs, it is still unclear how a BBH evolves. In evolution of supermassive black holes in galactic nuclei, BBHs may form and influence their host galaxies. In the final stage of a BBH, the gravitational radiation becomes efficient to remove the angular momentum of the BBH. To reach this stage, the angular momentum must be lost while its loss by dynamical friction is expected to slow down due to depletion of stars on orbits intersecting the BBH. As a possible scenario, a mass transfer from a circumbinary disk to each BH is suggested to add the angular momentum loss.[16] Furthermore, by combining the theoretical and observational studies, about 10% of nearby AGNs with $10^{6.5-7}\,M_{\odot}$ are estimated to be BBHs.[17] If so, there is a good chance to detect a binary signature. In fact, the optical observation of the blazer OJ287 over 100 years has revealed periodic bursts every ∼12 years and it is believed to be a BBH.[18]

The ORBIS mission is a special satellite dedicated to this science theme. It will observe only one or two specific AGNs in order to find out a binary motion. Such an observation focused on a limited target is unrealistic in large x-ray astronomy satellites. Even with all-sky x-ray monitors, a nearly continuous observation of one target is not easy, because all-sky x-ray monitors usually scan a part of the sky by narrowing the field of view with slits.[19] Therefore, the ORBIS can be a unique satellite complementary to large x-ray observatories and existing all-sky monitors.

Figure 2 overviews the ORBIS satellite and its science payload. Specifications are summarized in Table 1. It is 50 cm on a side with a mass of 50 kg including the science payload. Science requirements are shown in Table 2. A point source sensitivity comparable to an existing large all-sky x-ray monitor MAXI[19] is required. To achieve this sensitivity under the limited resources (size, weight, and power), focusing the incident x-rays at a low-background detector is essential. Therefore, a compact x-ray imaging spectrometer composed of the MEMS x-ray optic

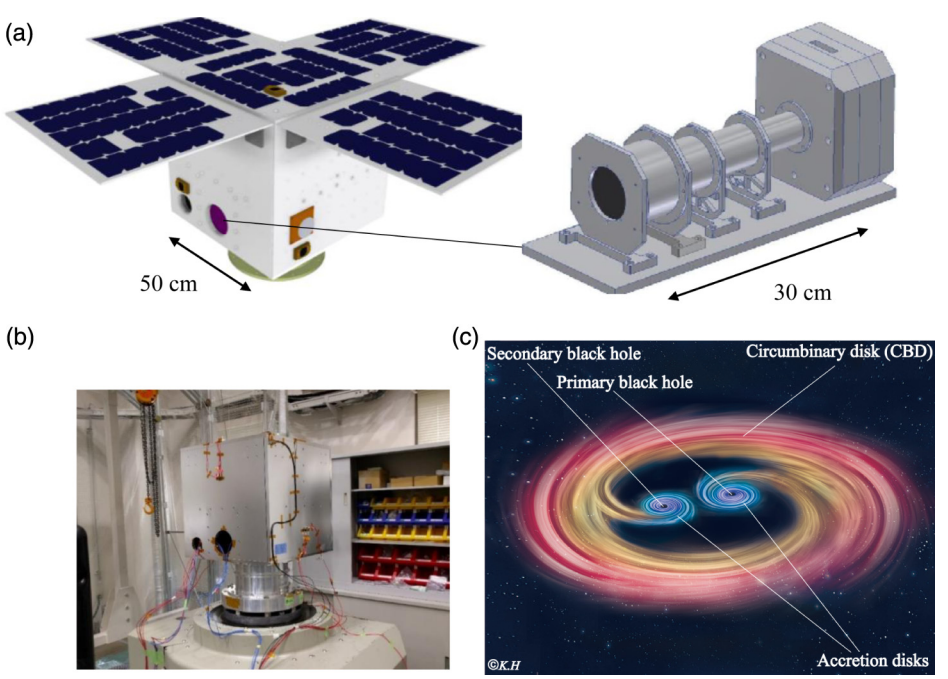

Fig. 2 Overview of the ORBIS mission: (a) three-dimensional cad drawings of the spacecraft and the payload, (b) a photo of a structure and thermal model,[15] and (c) artistic impression of a BBH.[17]

Table 1 Specifications of the ORBIS satellite.

	Unit	Values
Size	mm	$500 \times 500 \times 500$
Mass	kg	50
Power	W	144 (max)
Transmitter	kbps	100 (max) @ S-band
Receiver	kbps	1 (max) @ S-band
Altitude		550 km, low Earth orbit

Table 2 Requirements and specifications of the science payload in ORBIS.

	Unit	Values
Energy	keV	0.3 to 10
Point source sensitivity (3σ)	mCrab	5 in 3 days exposure
MEMS Wolter type-I x-ray optic		
Diameter	mm	100
Focal length	mm	250
Angular resolution	arcmin	<10
Mirror weight[a]	g	5/30
CCD detector		
Pixel size	μm	24×24
Format	pix	320×256
Area	mm	7.680×6.114
Energy resolution	eV	180 at 6 keV
Operating temperature	°C	−90

[a]Without/with an Al frame.

and the CCD detector will be onboard. The MEMS x-ray optic can be an ultralightweight telescope enabling a good angular resolution even at the required short focal length (<30 cm). The x-ray CCD is a miniature of the Hitomi SXI.[20]

We have constructed a structure and thermal model of the satellite. Environmental tests for this satellite model are ongoing. In parallel, a vibration test for the MEMS Wolter type-I optic has been conducted and no damage on the optic was observed. We have started an assembly of a part of the flight model of the satellite. The payload will be assembled in the satellite in 2019. An aimed launch year is around 2020. A piggy back launch by a JAXA H-IIA rocket is considered. A candidate for the science observation is a Seyfert 1 galaxy NGC 4151, which is suggested as a BBH candidate from an optical spectroscopy[21] and brightness in x-rays. Other candidates such as a blazer Mrk 421 are under investigation. The line of sight direction is constrained by an observational date and a solar angle. We will finalize the target when a launch date is fixed.

2.2 *GEO-X*

GEO-X (GEOspace x-ray imager) is a small exploration satellite under concept study by Tokyo Metropolitan University, Nagoya University, University of Tokyo, ISAS/JAXA, Hokkaido University, Kanto Gakuin University, Kobe University, and Tohoku University. Its objective is x-ray imaging of the Earth's magnetosphere using solar wind charge exchange emission from a location outside the magnetosphere. For this purpose, the satellite will be located at the vicinity of the Moon which is about 60 R_{Earth} from the Earth and will observe this emission from that distant place for the first time.

The solar wind charge exchange emission around the Earth was discovered with ROSAT during the all-sky survey.[22] It occurs between solar wind ions and exospheric neutrals near the Earth. The solar wind ion, such as O^{7+}, strips an electron from the neutral atom or molecule, such as H. The transferred electron to the ion decays into the ground state emitting photons as emission lines in the UV and x-ray wavelength range. Due to good energy resolution CCDs onboard Chandra, XMM-Newton, and Suzaku, it is now established as a time-variable foreground emission for x-ray astronomy satellites orbiting around the Earth.[23–27]

Because these large x-ray observatories have relatively small FOVs (e.g., 20 arcmin × 20 arcmin) and basically fly within the magnetosphere, fundamental questions such as how this emission is distributed and how this emission becomes bright are still unclear. Understanding of the solar wind charge exchange emission around the Earth is closely related to how the charge exchange emission occurs in other space environments such as supernova remnants and clusters of galaxies. Furthermore, from the viewpoint of planetary and magnetospheric science, this emission can be a new diagnostic tool to image the invisible Earth's magnetosphere.[28]

Many model studies have been conducted on this x-ray emission using magnetohydrodynamics (MHD) simulations of the Earth's magnetosphere. The x-ray emission is predicted to be strong at the dayside sheath region where both solar wind density and exospheric density are high. Magnetosheath, cusps, and bowshock can be visualized via x-rays (e.g., Ref. 29). These dayside regions of the magnetosphere are especially of importance in the context of interactions between solar wind and the magnetosphere. To date, precise measurements of electromagnetic fields and plasmas have been done by *in situ* observations. X-rays can be a new tool to take a global picture of the magnetosphere. Since the emission is expected to be associated with the magnetosphere, we basically need to escape from the magnetosphere.

GEO-X is a small satellite focusing on this special science theme. It will carry a wide FOV X-ray imaging spectrometer to map the emission with high sensitivity in 0.3 to 2 keV where the solar wind charge exchange emission is most strong as emission lines from ionized C, N, O, Fe, Mg, and S. The line of sight direction will be always toward the subsolar side of the Earth, i.e., near the dayside of the Earth. The satellite will be injected into high Earth orbit, outside the Earth's magnetosphere where the emission comes from. Similar to ORBIS, such observations have not been conducted.

Figure 3 shows a concept of the GEO-X satellite. Tables 3 and 4 summarize specifications of the satellite and the payload.

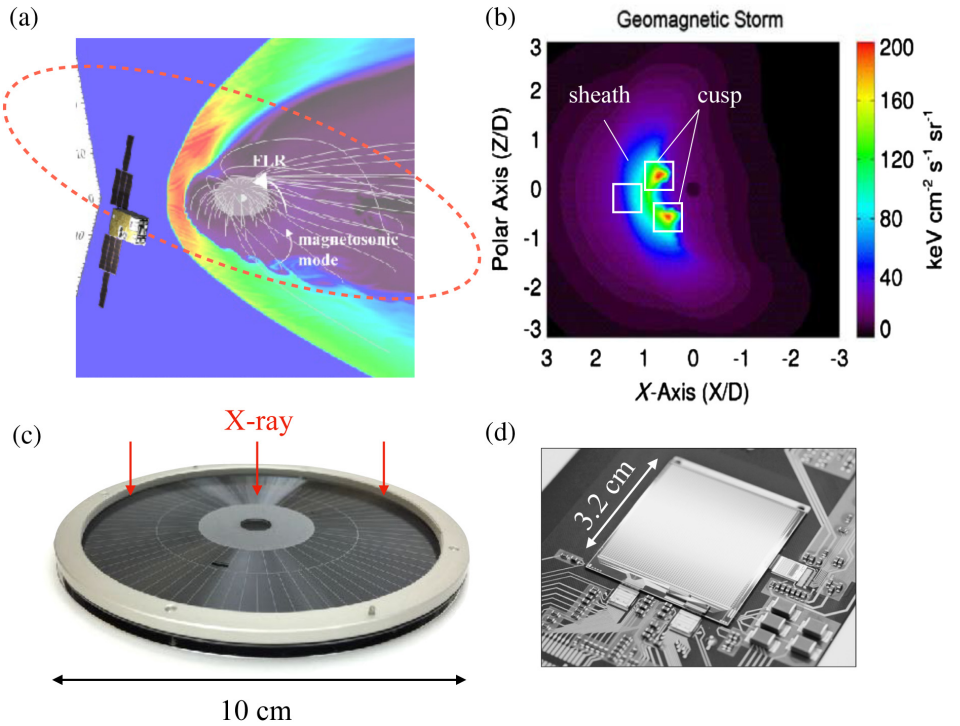

Fig. 3 Overview of the GEO-X mission: (a) a concept of the spacecraft orbiting around the Earth's magnetosphere,[30] (b) an MHD-based model for the solar wind charge exchange emission as observed from 50 R_{Earth},[29] (c) an MEMS Wolter type-I optic, and (d) a DepFET detector.[31] Each solid square in the MHD simulation indicates a FOV of the payload.

Table 3 Specifications of the GEO-X satellite under concept study. Numbers are to be determined.

	Unit	Values
Size	mm	$\sim 200 \times 200 \times 300$
Mass	kg	~30
Power	W	~100 (max)
Transmitter	kbps	~50 @ S-band
Receiver	kbps	~1 @ S-band
Altitude		~40 to 60 R_{Earth}, high Earth orbit

Table 4 Requirements and specifications of the science payload in GEO-X.

	Unit	Values
Energy	keV	0.3–2
Grasp	$\mathrm{cm}^2\,\mathrm{deg}^2$	10 at 0.6 keV
MEMS Wolter type-I x-ray optic		
Diameter	mm	100
Focal length	mm	250
Angular resolution	arcmin	<10
Mirror weight[a]	g	5/30
DepFET detector		
Pixel size	μm	300×300
Format	pix	64×64
Area	mm	19.2×19.2
Energy resolution	eV	80 at 1 keV
Operating temperature	°C	−60

[a]Without/with an Al frame.

The satellite will be a ~12 U cubesat or a similar size. It will be injected into a near circular high Earth orbit with an altitude of $40 - 60\,R_{\mathrm{Earrth}}$, i.e., near the Moon and a small inclination angle. A propulsion system composed of N_2O and polyethylene can be attached to the satellite. The weight of the satellite will be ~30 kg and the proplusion system will add ~20 kg. In total, the satellite including the proplusion system will be ~50 kg or less. A piggy back launch of the JAXA's HII-A or HIII rocket is considered. Necessary Δv depends on the rocket and its orbital insertion but it will be at most $\sim 400 - 500$ m/s when the satellite is first injected into an elliptical orbit by the rocket with an apogee of ~60,000 km.

To achieve a good sensitivity to this diffuse x-ray emission, a grasp or a multiple of an effective area and FOV is important. GEO-X will achieve a large grasp comparable to the Suzaku X-ray CCD and telescope system in this small satellite platform. It is in principle possible because of its short focal length and operation in the soft x-ray band, resulting in a large FOV of 4 deg ×4 deg at least. The required angular resolution is

moderate because the x-ray emission is expected to be widely extended. The same Wolter type-I design as in ORBIS will be adopted, allowing us swift development. The aimed launch year is around 2022, near the next solar maximum.

We have estimated the number of events that GEO-X will detect using past solar wind data taken with the GOES and ACE satellites during 1998 to 2011. This duration covers one solar cycle. Here, we assumed that signals are proportional to an incoming ion flux, while the background is a combination of soft x-ray sky background and non-x-ray background. For simplicity, we focused on the $O^{6+}K_\alpha$ band (0.5 to 0.6 keV). From Ref. 29, the x-ray flux at a certain solar wind O^{7+} flux level can be estimated. The soft x-ray background and the instrumental background including a radiation noise mainly due to high energy protons were calculated from the past x-ray observations[32] and our GEANT4 simulations.[33]

Figure 4 shows the results. We counted how many data points can meet the S/N ratio >20 based on the solar wind data and the past x-ray astronomy observations. The number of the data points can be converted to an estimated observational duration in which the high S/N ratio is expected. The estimated number of such data points peaks around the solar maximum and decreases toward the solar minimum. At the solar maximum, ~150 data points exist. Because each datum is averaged over 2 h, this indicates that we can obtain ~300 data sets having $S/N > 20$ at the 1-h exposure time in a single year with GEO-X. Even at a 10-min exposure, good data points exist. On the other hand, at the solar minimum, the number of the data points is nearly zero. Therefore, the launch year is crucial. The most proper launch year would be the early 2020's in which the solar activity will rise.

For the same purpose, i.e., x-ray imaging of the Earth's magnetosphere, the SMILE and CuPID missions are planned in ESA-China and the USA, respectively.[34,35] The SMILE mission is a medium-class satellite observing the solar wind charge exchange emission from an elliptical orbit with an apogee of $\sim 20\,R_{\mathrm{Earth}}$. The orbit has a high inclination angle to observe UV aurora at the same time. Wide FOV Lobster MCP optics and a large format CCD will be onboard. The CuPID mission is a 6U cubesat at low Earth orbit and will carry Lobster MCP optics and an MCP detector. In contrast, GEO-X will observe this emission from the most distant place with a relatively small inclination angle, allowing unique sideview imaging of the Earth's magnetosphere. Also the DepFET detector is not significantly affected for optical light contamination, enabling observations of cusps near the dayside of the Earth. These features will make GEO-X unique and complementary to the other missions.

3 MEMS X-Ray Optics

3.1 *Concept*

We utilize micromachining techniques for fabrication of the micropore x-ray optics. We have tested various techniques including anisotropic wet etching, deep reactive ion etching (DRIE), x-ray LIGA (Lithographie, Galvanik, und Abformung) and focused ion beam, and succeeded to verify x-ray reflection on sidewalls of micropores.[9,10,14] Now we focus on the DRIE-fabricated optics. The process flow is shown in Fig. 5.

Sidewalls of curvilinear micropores made by DRIE are smoothed by hydrogen annealing at $>1000C^{\circ}$. The wafer is deformed to a spherical shape by hot plastic deformation. Sidewalls can be coated with a high-Z material by atomic layer deposition (ALD). Two wafers deformed to different curvature radii are precisely stacked to form a Wolter type-I optic. Because of the tiny pores and thin wafers, this type of optics can be the lightest x-ray telescope ever achieved. It is also low cost because we basically fabricate the optics by ourselves.

A conical approximation of the Wolter type-I is almost negligible, ~2 arcsec, even at a short focal length of 25 cm when the wafer thickness is 300 μm and the reflection angle is 1 deg. A theoretical limit on the angular resolution is an x-ray diffraction within each micropore which is ~13 arcsec at 1 keV when the

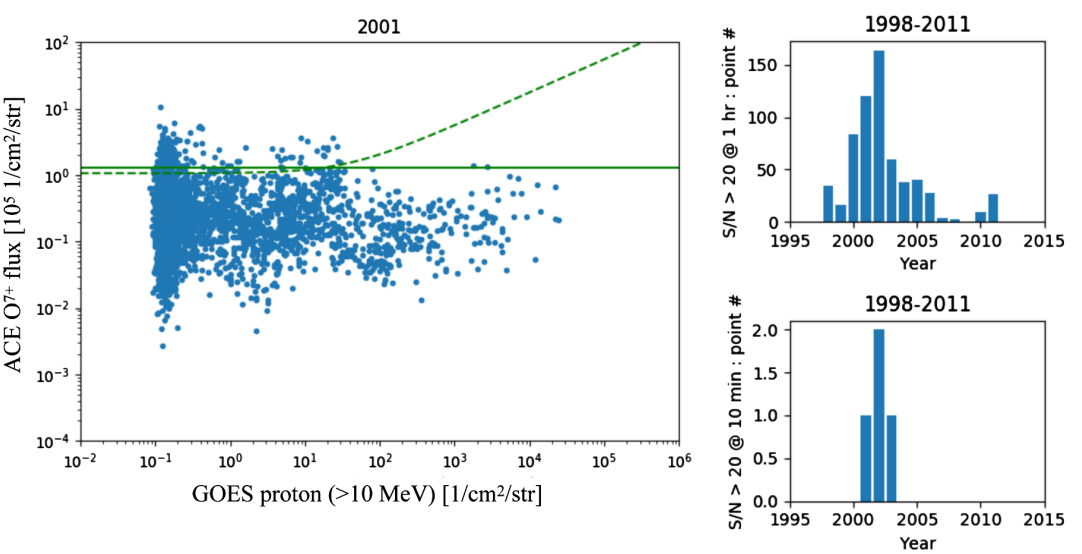

Fig. 4 Example of GOES proton (>10 MeV) flux versus ACE O^{7+} flux in 2001, where each data point is 2 h average. Solid and dashed lines indicate boundaries of the data points having signal-to-noise ratios $(S/N) > 20$ when photon statistics or background fluctuation is considered, respectively. GEO-X instrumental parameters and an exposure time of 1 h is assumed. On the right side, histograms of the number of points having $S/N > 20$ in the 1 h or 10 min exposure are plotted as a function of year from 1998 to 2011.

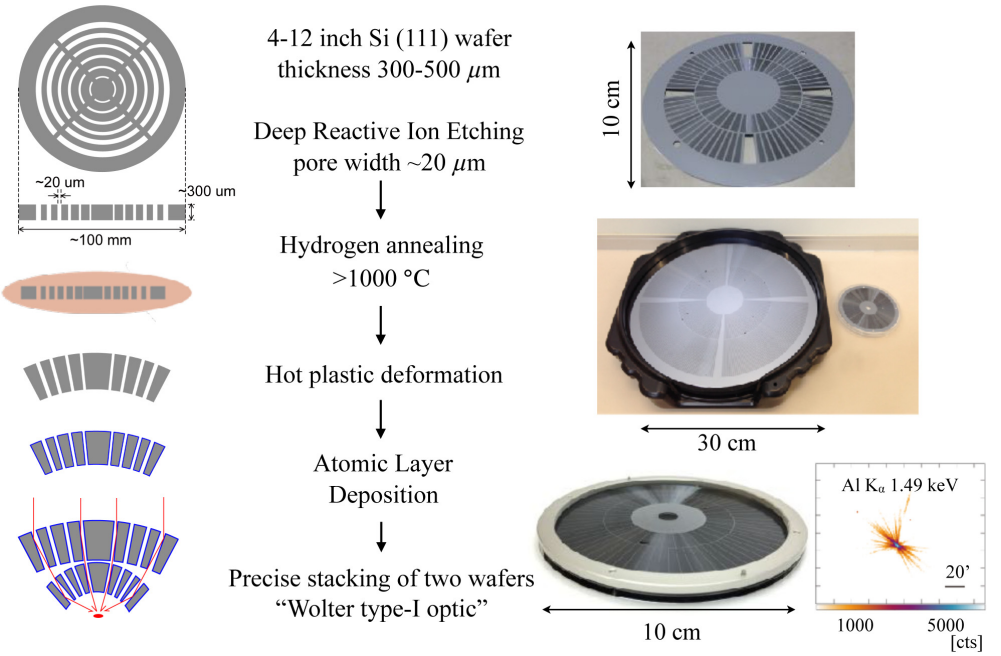

Fig. 5 Process flow of the MEMS x-ray optics. From top to bottom, photos show a single-stage 4-in. Si optic, a 12-in. Si optic, and a 4-in. Wolter type-I optic.

micropore width is 20 μm. Therefore, an ultralightweight telescope with an angular resolution better than 1 arcmin would be possible. We have verified x-ray reflection and imaging with this method as shown in Fig. 5.

3.2 *Design*

Table 5 summarizes the baseline design of the MEMS Wolter type-I optic for ORBIS and GEO-X. The optic will be made from 4-in. Si wafers. An open area ratio will be ~20%. Sidewalls will be coated by Pt. A thin Al_2O_3 layer will be between Si and Pt for good adhesion. Figure 6 shows raytracing simulations based on these parameters. A photon number for each simulation is 50,000. A detector size of 20 mm × 20 mm is used considering the GEO-X configuration. A microroughness of each mirror is assumed as 1 nm in rms from the experiments. The focused image changes depending on the incident angle due to vignetting and stray light. We estimate an effective area and a grasp by integrating a circular area around the focus with a radius of 1.5 mm corresponding to 20 arcmin on the detector. Figure 7 shows the obtained results.

In ORBIS, the on-axis effective area is crucial because the target is a point source and the line of sight direction will be always toward the target. A moderate effective area of ~3 cm^2 is expected at 1 keV. Here, the detector quantum efficiency and the optical blocking filter of the Hitomi SXI are assumed. This value is a factor of ~100 smaller than that of Suzaku XIS. However, the sensitivity to the point source is proportional to a square root of the effective area and the exposure time when the photon statistics or the background noise dominates. Therefore, because of the observation strategy whereby only a specific target is observed, the required sensitivity of 5 mCrab in three days exposure time can be achieved as far as the background level is similar to the Suzaku XIS. We expect to achieve such a low background in ORBIS because the orbit and the detector shield will be similar to those in Suzaku.

Table 5 Baseline design of the MEMS Wolter type-I optics for ORBIS and GEO-X.

	Unit	Values
Wafer properties		
Diameter	mm	100
Thickness	μm	300
Curvature radius	mm	1000 (first), 333 (second)
Micropore properties		
Micropore width	μm	20
Space between micropores	μm	20
Innermost radius	mm	15
Outermost radius	mm	45
Sidewall coating		$Pt + Al_2O_3$
Required performance		
Angular resolution	arcmin	10
Effective area	cm^2	3 at 1 keV
Grasp	$cm^2\ deg^2$	10 at 0.6 keV

In GEO-X, the grasp is more important. Because of the large field of view, the grasp will be comparable to, or even better than, that of the Suzaku XIS. The calculated value is 1500 $mm^2\ deg^2$ or 15 $cm^2\ deg^2$ at 0.6 keV. After considering the detector and optical blocking filter efficiency, which will be similar to ORBIS (~70% at 0.6 keV and >90% above

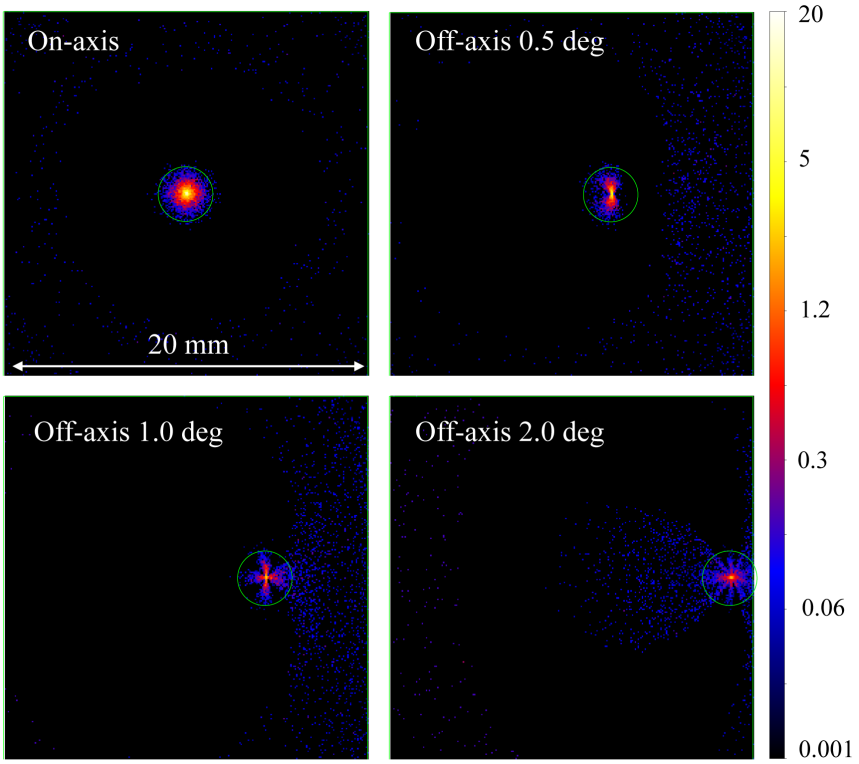

Fig. 6 Raytracing results for the MEMS Wolter type-I optic assuming optics parameters in Table 5 at 0.6 keV. Different incident angles are used. A color scale is in arbitrary unit. A solid circle corresponds to an area with a radius of 1.5 mm used for the effective area and grasp calculations.

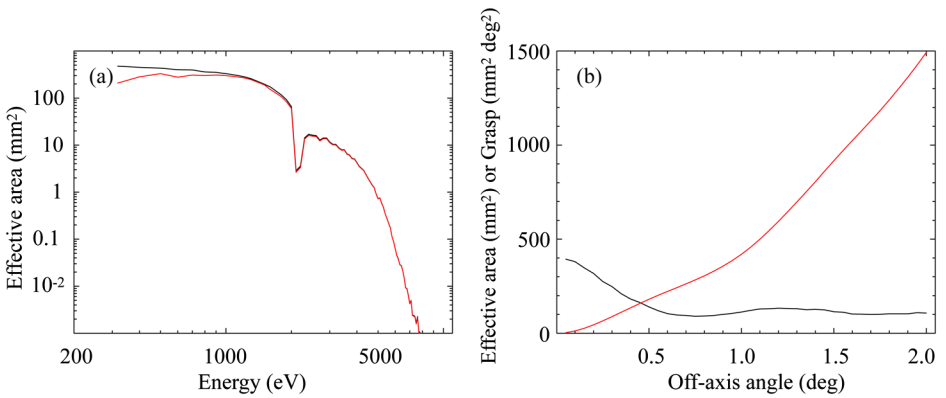

Fig. 7 (a) Effective area of the MEMS Wolter type-I optic estimated from the raytracing simulations. Black and red curves represent an effective area without and with a detector quantum efficiency and an optical blocking filter. (b) Grasp of the MEMS Wolter type-I optic as a function of off-axis angle. Black and red curves are an effective area and a grasp. The detector and optical blocking filter efficiency is not included.

1 keV), the required grasp of >10 cm^2 deg^2 will be satisfied. Thus, these simulations indicate that the compact and light weight MEMS Wolter type-I optic can meet the required sensitivity in ORBIS and GEO-X under the very limited resources of these small missions.

3.3 *Recent Development*

We show our recent development of the MEMS x-ray optics toward ORBIS and GEO-X. As described above, we have demonstrated the Wolter type-I optic. We are now improving the optics performance including the angular resolution and the effective area.

3.4 *Angular Resolution*

From a series of evaluations of mirror qualities and arrangement errors in a step by step manner at individual processes, we now consider that one of the major factors for the angular resolution is mirror quality itself. Figure 8(a) shows our recent x-ray test of a single mirror. It has a relatively sharp peak with a half energy width of $\sim$5 arcmin on average within the optic. A typical FWHM is $\sim$3 arcmin. The required angular resolution by single reflection is 5 arcmin in both ORBIS and GEO-X. Therefore, this main component meets the requirement.

However, there are two other components that should be eliminated or reduced. One is a broad component represented

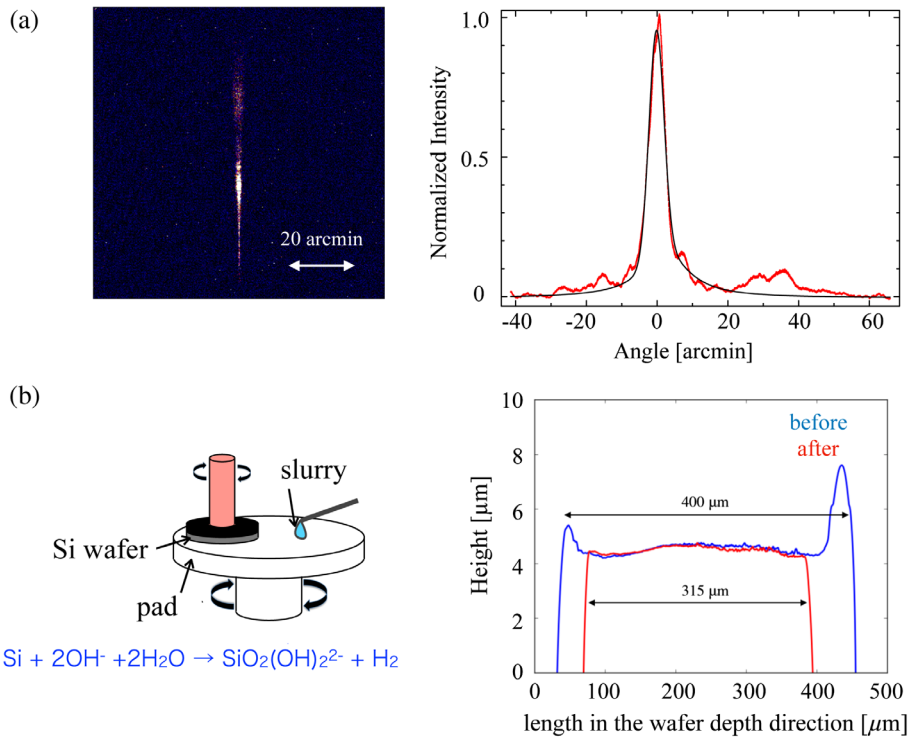

Fig. 8 (a) X-ray response of a single mirror after DRIE and annealing at AlK$_\alpha$1.49 keV and its projected profile fitted with Gaussian and Lorentzian models. (b) Concept of chemical mechanical polishing and an example of sidewall profiles of a sample DRIE-fabricated optic before and after polishing.

by a Lorentzian model. A half energy width of this component is typically ~15 arcmin. As a result, the half energy width of the single mirror can become ~10 arcmin. The angular distribution of the Lorentzian component is similar to expected x-ray scattering from the mirror surface power spectrum density (PSD). Therefore, we are now trying to suppress the surface roughness by changing DRIE and annealing processes. Because the x-ray scattering intensity is proportional to the PSD and the rms roughness is an integral of the PSD in the frequency domain, we aim at a factor of ~3 reduction of the rms roughness which leads to a factor of ~9 reduction of the scattering intensity if this is the case.

The other unwanted component is an additional peak located at large reflection angles. It is most likely due to edge structures in the sidewalls generated after DRIE. We thus newly introduced chemical mechanical polishing of the wafer after DRIE from both sides. We filled micropores with photoresist, in order not to break structures, and removed the photoresist after polishing. As shown in Fig. 8(b), we succeeded in removing the edge structures without destruction of the wafer. In addition to removing the edge structure, this process allows us to leave the flat mirror surface. Thus, we can expect not only a large effective area at small reflection angles, but also a better angular resolution.

3.5 *Effective Area*

In addition to the angular resolution, we tested a new ALD process to increase the effective area.[36] Coating of the sidewalls with high Z materials is necessary in the MEMS x-ray optics. Since a standard coating process such as sputtering or evaporation do not allow conformal coating of the high aspect sidewalls, we selected the ALD as a new coating method. We tested Ir ALD in the early stage of our development.[37] Although the coating was successful in terms of x-ray reflectivity, the cost was higher.

Hence, we recently tried Pt ALD. It consists of two reactions. At first, we introduce a Pt precursor 2(MeCp) $PtMe_3$. Then, the precursor attached to the wafer surface is catalytically combusted by O_2. By cycling these two reactions, a pure Pt layer can be coated on the Si sidewalls. The reaction temperature and the growth rate are ~270°C and ~0.4 Å/cycle, respectively. To strengthen adhesion, we inserted an Al_2O_3 layer between Si and Pt.

Figure 9 shows an example of the MEMS x-ray optic after DRIE, annealing, and ALD. Aimed thicknesses of Pt and Al_2O_3 layers were 20 and 10 nm, respectively. A transmission electron microscope image of a sidewall indicates that the two layers are coated properly on the sidewall with Pt and Al_2O_3 thicknesses of 25 and 12 nm, respectively. At Al K$_\alpha$1.49 keV, an enhanced x-ray reflectivity was confirmed. However, the surface roughness estimated from the curves seemed to increase after coating from 1.6 to 2.2 nm rms. A required microroughness in ORBIS and GEO-X is about <2 nm in rms.

Therefore, we coated another wafer with a different ALD method. To activate chemical reactions, we introduced O plasma instead of O_2 gas. This process is called plasma ALD and distinguished from the previous process, thermal ALD. The aimed thicknesses of the two layers are the same as before. Consequently, the plasma ALD-coated sample showed thicknesses similar to those in the thermal ALD but a better reflectivity, while the surface roughness before coating was the same as that before the thermal ALD. No significant change in the microroughness was observed. The required microroughness in ORBIS and GEO-X is below ~1.5 nm rms. Therefore, these results support the view that the Pt coating by ALD is usable for ORBIS and GEO-X.

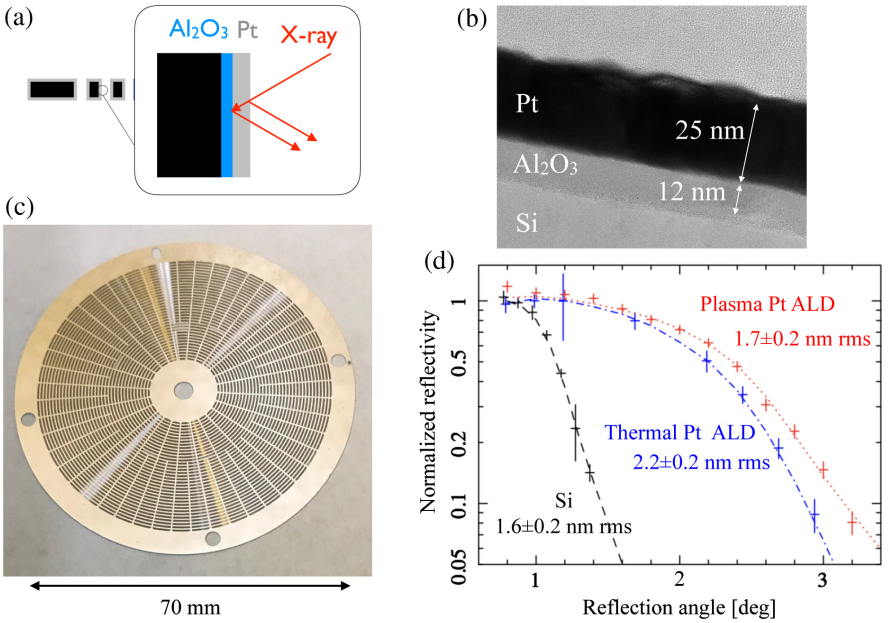

Fig. 9 (a, c) Concept and photo of Pt-coated MEMS x-ray optics, (b) a transmission electron microscope image of a sidewall, and (d) x-ray reflectivity curves at AlK$_\alpha$1.49 keV of the sidewalls. The photo and electron microscope image are for the plasma Pt ALD sample, while the reflectivity curves are for both the thermal and plasma Pt ALD samples. Numbers indicate microroughness estimated from the reflectivity curves.

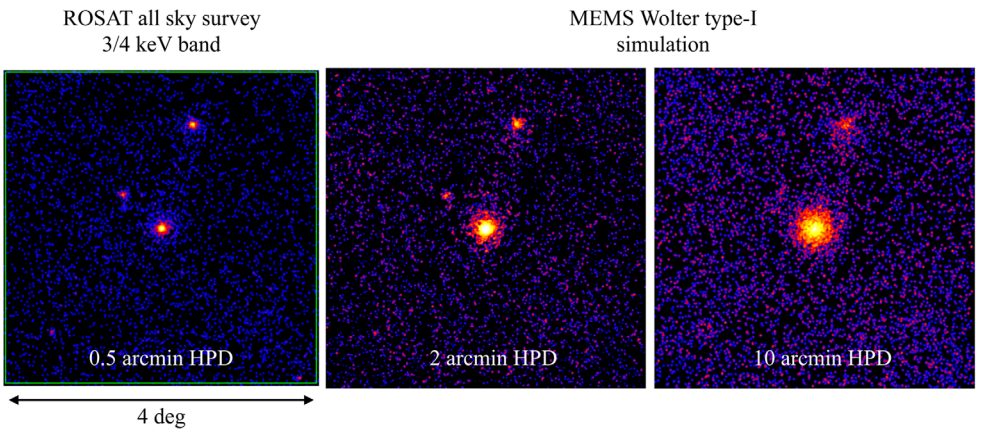

Fig. 10 MEMS Wolter type-I simulations compared to an original ROSAT all-sky survey 3/4 keV band image near the Galactic center (ra, dec) = (266.404996, 28.936172) in J2000.[38] The parameters for the MEMS Wolter type-I optic are summarized in Table 5. An x-ray energy of 0.6 keV is assumed. The exposure time of the original ROSAT image is ~290 s, while the assumed exposure time for each MEMS Wolter type-I simulation image is set at ~8 ks.

We plan to start fabricating the flight model Wolter type-I optics for ORBIS GEO-X soon. New technologies under testing to improve the angular resolution and the effective area are promising. In parallel, shock and thermal tests for a test optic will be conducted. We hope to finish all these development items within the schedule and launch the two optics in the early 2020s.

4 Summary

To summarize, future small missions such as ORBIS and GEO-X need new ultralightweight telescopes with a moderate angular resolution at a short focal length and/or a wide field of view. Our MEMS x-ray optics are ideal for these purposes. We have demonstrated x-ray reflection and imaging with this method. Now we are improving the angular resolution and the effective area by introducing new cutting edge technologies. We hope to verify this new telescope in ORBIS and GEO-X, and then with other small or medium satellite missions as well as solar system explorations to Jupiter or Mars in the late 2020s, Fig. 10 shows simulated images using an ROSAT all-sky survey 3/4 keV band image near the Galactic center. Our final goal is to achieve angular resolution comparable to the ROSAT all-sky survey.

Acknowledgments

The authors acknowledge Yosuke Matsumoto and Masaki Numazawa for their help in MHD and raytracing simulations,

respectively. This work was supported by MEXT KAKENHI Grant Nos. 20684006, 23684009, and 26287032, Toray Science and Technology Grant, and MEXT promotion grant for aerospace science. This paper is based on the SPIE proceedings paper 10699-30 from Astronomical Telescopes + Instrumentation 2018.

References

1. M. Bavdaz et al., "Development of x-ray optics for the XEUS Mission," *Proc. SPIE* **5539**, 95–103 (2004).
2. M. Bavdaz et al., "The ATHENA telescope and optics status," *Proc. SPIE* **10399**, 103990B (2017).
3. W. W. Zhang et al., "Monocrystalline silicon and the meta-shell approach to building x-ray astronomical optics," *Proc. SPIE* **10399**, 103990S (2017).
4. V. Cotroneo et al., "Thermal forming of glass substrates for adjustable optics (Conference Presentation)," *Proc. SPIE* **10399**, 103990Y (2017).
5. Y. Ezoe, M. Koshiishi, and K. Mitsuda, "MEMS open the way to ultra-lightweight and low-cost x-ray optics," *SPIE Newsroom* (2006), http://spie.org/x8595.xml.
6. S. W. Wilkins et al., "On the concentration, focusing, and collimation of x-rays and neutrons using microchannel plates and configurations of holes," *Rev. Sci. Instrum.* **60**, 1026–1036 (1989).
7. M. Bavdaz et al., "X-ray pore optics technologies and their application in space telescopes," *X-Ray Opt. Instrum.* **2010**, 1–15 (2010).
8. G. W. Fraser et al., "The mercury imaging x-ray spectrometer (MIXS) on bepicolombo," *Planet. Space. Sci.* **58**, 79–95 (2010).
9. Y. Ezoe et al., "Micropore x-ray optics using anisotropic wet etching of (110) silicon wafers," *Appl. Opt.* **45**, 8932–8938 (2006).
10. Y. Ezoe et al., "Ultra light-weight and high-resolution x-ray mirrors using drie and x-ray liga techniques for space x-ray telescopes," *Microsys. Technol.* **16**, 1633–1641 (2010).
11. H. Yamaguchi et al., "Magnetic field assisted finishing for micro-pore x-ray focusing mirrors fabricated by deep reactive ion etching," *CIRP Ann.* **59**, 351–354 (2010).
12. R. Riveros et al., "Development of an alternating magnetic field assisted finishing process for mems micro-pore x-ray optics," *Appl. Opt.* **49**, 3511–3521 (2010).
13. Y. Ezoe et al., "Large aperture focusing of x-rays with micro pore optics using dry etching of silicon wafers," *Opt. Lett.* **37**, 779–781 (2012).
14. M. Numazawa et al., "First demonstration of x-ray mirrors using focused ion beam," *Jpn. J. Appl. Phys.* **55**, 06GP11 (2016).
15. J. Matsushima et al., "Development of binary black hole observation satellite 'ORBIS'," *Trans. Jpn Soc. Astron. Space Sci.*.
16. K. Hayasaki, "A new mechanism for massive binary black-hole evolution," *Publ. Astron. Soc. Jpn.* **61**, 65–74 (2009).
17. K. Hayasaki, Y. Ueda, and N. Isobe, "Mass function of binary massive black holes in active galactic nuclei," *Publ. Astron. Soc. Jpn.* **62**, 1351–1360 (2010).
18. M. J. Valtonen, "New orbit solutions for the precessing binary black hole model of oj 287," *Astrophys. J.* **659**, 1074–1081 (2007).
19. T. Mihara et al., "Gas slit camera (GSC) onboard MAXI on ISS," *Publ. Astron. Soc. Jpn.* **63**, S623–S634 (2011).
20. H. Nakajima et al., "In-orbit performance of the soft X-ray imaging system aboard Hitomi (ASTRO-H)," *Publ. Astron. Soc. Jpn.* **70**, 21 (2018).
21. E. Bon et al., "The first spectroscopically resolved sub-parsec orbit of a supermassive binary ck hole," *Astrophys. J.* **759**, 118 (2012).
22. S. L. Snowden et al., "Analysis procedures for ROSAT XRT/PSPC observations of extended objects and the diffuse background," *Astrophys. J.* **424**, 714–728 (1994).
23. R. Fujimoto et al., "Evidence for solar-wind charge-exchange x-ray emission from the Earth's magnetosheath," *Publ. Astron. Soc. Jpn.* **59**, S133–S140 (2007).
24. J. A. Carter and S. Sembay, "Identifying XMM-Newton observations affected by solar wind charge exchange. Part I," *Astron. Astrophys.* **489**, 837–848 (2008).
25. Y. Ezoe et al., "Time variability of the geocoronal solar-wind charge exchange in the direction of the celestial equator," *Publ. Astron. Soc. Jpn.* **62**, 981–986 (2010).
26. Y. Ezoe et al., "Enhancement of terrestrial diffuse x-ray emission associated with coronal mass ejection and geomagnetic storm," *Publ. Astron. Soc. Jpn.* **63**, S691–S704 (2011).
27. K. Ishikawa et al., "Suzaku observation of strong solar-wind charge-exchange emission from the terrestrial exosphere during a geomagnetic storm," *Publ. Astron. Soc. Jpn.* **65**, 63 (2013).
28. D. G. Sibeck et al., "Imaging plasma density structures in the soft x-rays generated by solar wind charge exchange with neutrals," *Space Sci. Rev.* **214**, 79 (2018).
29. I. P. Robertson et al., "X-ray emission from the terrestrial magnetosheath including the cusps," *J. Geophys. Res.* **111**, A12105 (2006).
30. R. Funase and E. P. Team, "EQUULEUS: a 6U CubeSat to Fly to Earth—Moon Lagrange Point onboard SLS EM-1," in *LCPM-12* (2017).
31. J. Treis et al., "MIXS on BepiColombo and its DEPFET based focal plane instrumentation," *Nucl. Instrum. Methods A* **624**, 540–547 (2010).
32. T. Yoshino et al., "Energy spectra of the soft x-ray diffuse emission in fourteen fields observed with Suzaku," *Publ. Astron. Soc. Jpn.* **61**, 805–823 (2009).
33. S. Kasahara et al., "Radiation background and dose estimates for future x-ray observations in the Jovian magnetosphere," *Planet. Space Sci.* **75**, 129–135 (2013).
34. ESA, "The SMILE mission," http://sci.esa.int/smile/.
35. CuPID, "The CuPID mission," Boston University, Mechanical Engineering, http://sites.bu.edu/cupid/.
36. K. Takeuchi et al., "Pt thermal atomic layer deposition for silicon x-ray micropore optics," *Appl. Opt.* **57**, 3237–3243 (2018).
37. T. Ogawa et al., "Iridium-coated micropore x-ray optics using dry etching of a silicon wafer and atomic layer deposition," *Appl. Opt.* **52**, 5949–5956 (2013).
38. J. Englhauser, "The ROSAT X-ray All-Sky Survey," http://www.xray.mpe.mpg.de/cgi-bin/rosat/rosat-survey (12 April 2001).

Yuichiro Ezoe is an associate professor at Tokyo Metropolitan University. He received his BS, MS, and PhD degrees in physics from the University of Tokyo in 1999, 2001, and 2004, respectively. He is the author of more than 100 journal papers and has written one book chapter. His current research interests include x-ray optics, low temperature detectors, and x-ray emission from various objects including solar system objects, nearby stars having exoplanets, massive star forming regions and blackholes.

Hironori Sahara received his PhD at the Department of Aeronautics and Astronautics of University of Tokyo in 1999. He was a fellow at the National Aerospace Laboratory of Japan from 2000 to 2003. He was a research associate at the University of Tokyo from 2004 to 2007. He was an associate professor at the Department of Aeronautics and Astronautics in Tokyo Metropolitan University, and has been a professor since 2016.

Graziella Branduardi-Raymont received his physics degree from the University of Milano, Italy, and his PhD in x-ray astronomy, University College London (UCL). He is a postdoctoral researcher, Harvard-Smithsonian Center for Astrophysics, USA, and then UCL Mullard Space Science Laboratory. Currently, he is a UCL professor of space astronomy. He participated in major x-ray observatory missions over four decades, He is the coinvestigator for the Reflection Grating Spectrometer operating on board the XMM-Newton observatory since 1999. He is the coleader of the joint ESA-Chinese Academy of Sciences SMILE mission due for launch in 2023.

Biographies for the other authors are not available.